

Peripheral Membrane Interactions Boost the Engagement by an Anti-HIV-1 Broadly Neutralizing Antibody.

Rujas, Edurne

Biofisika Institute (Consejo Superior de Investigaciones Científicas, UPV/EHU), and Department of Biochemistry and Molecular Biology, University of the Basque Country (UPV/EHU)

Caaveiro, José M. M.

Department of Bioengineering, Graduate School of Engineering, University of Tokyo

Insausti, Sara

Biofisika Institute (Consejo Superior de Investigaciones Científicas, UPV/EHU), and Department of Biochemistry and Molecular Biology, University of the Basque Country (UPV/EHU)

García-Porras, Miguel

Biofisika Institute (Consejo Superior de Investigaciones Científicas, UPV/EHU), and Department of Biochemistry and Molecular Biology, University of the Basque Country (UPV/EHU)

他

<https://hdl.handle.net/2324/1812333>

出版情報 : The Journal of Biological Chemistry. 292, pp.5571-5583, 2017-03-31. Knickerbocker Press

バージョン :

権利関係 :



Peripheral Membrane Interactions Boost the Engagement
by an Anti HIV-1 Broadly Neutralizing Antibody.

**Edurne Rujas^{1,2}, José M. M. Caaveiro², Sara Insausti¹, Miguel García-Porras¹, Kouhei Tsumoto²,
and José L. Nieva¹**

¹Biofisika Institute (CSIC, UPV/EHU) and Department of Biochemistry and Molecular Biology,
University of the Basque Country, P.O. Box 644, 48080 Bilbao, Spain.

²Department of Bioengineering, Graduate School of Engineering, The University of Tokyo, Bunkyo-ku,
113-8656 Tokyo, Japan.

Running title: *Peripheral membrane interactions of an anti-HIV-1 antibody*

To whom correspondence should be addressed: Prof. Kouhei Tsumoto, Department of Bioengineering,
The University of Tokyo, Bunkyo-ku, 113-8656 Tokyo, Japan, Phone: +(81) 36 409 2129; E-mail:
tsumoto@k.u-tokyo.ac.jp; Prof. José L. Nieva, Department of Biochemistry and Molecular Biology,
University of the Basque Country (UPV/EHU), P.O. Box 644, 48080 Bilbao, Spain, Phone: +34 94 601
3353; Fax: +34 94 601 3360; E-mail: gbpniesj@lg.ehu.es

Key words: 4E10 antibody; broadly neutralizing antibody; human immunodeficiency virus (HIV); lipid
polyreactivity; MPER vaccine; protein-membrane interaction; vaccine development

ABSTRACT

The 4E10 antibody displays an extreme breadth of HIV-1 neutralization and therefore constitutes a suitable model system for structure-guided vaccine design and immunotherapeutics against AIDS. In this regard, the relevance of auto-reactivity with membrane lipids for the biological function of this antibody is still a subject of controversy. To address this dispute, herein we have compared the membrane-partitioning ability of the 4E10 antibody and several of its variants, which were mutated at the region of the paratope surface in contact with the membrane-interface. We first employed a physical separation approach (vesicle flotation), and subsequently carried out quantitative fluorescence measurements in an intact system (spectroscopic titration), using 4E10 Fab labeled with the polarity-sensitive 4-Chloro-7-Nitrobenz-2-Oxa-1,3-Diazole (NBD) probe. Moreover, recognition of epitope peptide in membrane was demonstrated by photo-cross-linking assays using a Fab that incorporated the genetically encoded unnatural amino acid p-benzoylphenylalanine (pBPA). The experimental data ruled out that the proposed stereospecific recognition of viral lipids was necessary for the function of the antibody. In contrast, our data suggest that nonspecific electrostatic interactions

between basic residues of 4E10 and acidic phospholipids in the membranes contribute to the observed biological function. Moreover, the energetics of membrane-partitioning indicated that 4E10 behaves as a peripheral membrane protein, tightening the binding to the ligand epitope inserted in the viral membrane. The implications of these findings for the natural production and biological function of this antibody are discussed.

Engagement by the 4E10 antibody of a conserved helical epitope on the membrane-proximal external region (MPER)¹ of the Env gp41 subunit results in one of the broadest neutralization levels of HIV-1 reported to date (98 % of viruses blocked in standard infectivity tests (1-3)). Prevalence of anti-MPER antibodies has been linked to neutralization breadth and potency of certain sera from chronically infected individuals (3,4). Thus, solving the molecular mechanism that leads to viral blocking after MPER engagement by broadly neutralizing antibody (bNAb) 4E10 is critical in the fields of vaccine design and immunotherapy (3,5-7). Since the viral membrane takes part in the stabilization of the MPER helix, it is generally accepted that antibodies targeting the MPER-membrane site are

polyspecific, showing capacity to bind lipid moieties (8-12). In that respect, anti-MPER antibodies have been proposed to resemble natural antibodies that bind to phospholipids (13). Furthermore, it has been argued that HIV-1 may have evolved to escape anti-MPER responses by structural mimicry of the phospholipid ligands bound to autoantibodies (14). Following this line of evidence, some researchers consider anti-MPER antibodies as generally auto-reactive, and postulate that their natural production is limited by B-cell tolerance mechanisms (14-16).

Some experimental evidence suggesting that bNAb 4E10 binds to phospholipids, particularly anionic species such as phosphatidylserine (PS), cardiolipin (CL) or phosphatidylinositol (PI), has been obtained in several laboratories during the last decade (9,10,14,17), which supported the notion of structural mimicry of phospholipid-binding sites by the antibody (13,14). In agreement with that idea, the existence of a binding pocket accommodating the polar head group of PS or CL within the paratope of 4E10 was proposed (10). Strikingly, the structure of the paratope with lipid bound would differ from that of the paratope with peptide epitope bound (10). Nonetheless, some of these concepts have been challenged by the recent resolution of crystal structures of the unbound Fab form (18,19) and Fab-lipid complexes (12,20).

In particular, Irimia *et al.* (12) determined the crystal structure of the complex between 4E10 Fab and lipids such as phosphatidic acid (PA), phosphatidylglycerol (PG), and the lipid moiety glycerol phosphate, which revealed two binding sites on the paratope surface in contact with the membrane interface. Lipid recognition occurred primarily at the heavy-chain complementarity determining region 1 (CDRH1) between the backbone atoms of the protein, and the glycerol and phosphate moieties which are the common components of phosphoglycerides. Thus, from these results it appears that the 4E10 Fab does not behave as a target-specific phospholipid-binding domain that performs selective-stereospecific recognition of ligand molecules (21). The crystallographic data were also consistent with the simultaneous accommodation of the phospholipid head-group moieties and the bound peptide epitope within the 4E10 paratope, and further underscored the role of the hydrophobic CDRH3

apex in establishing interactions with the lipid tails (12).

In an attempt to discern the role played by lipid interactions in the 4E10 neutralization mechanism, we have herein determined the specificity and intensity of its interactions with phospholipids in the context of biologically relevant bilayer systems. To that end, we have employed liposome-flotation assays (a physical separation method), which were subsequently complemented with spectroscopic titration assays using Fabs labeled with the polarity-sensitive probe NBD. Moreover, a Fab 4E10 variant incorporating the UV-sensitive unnatural amino acid *p*BPA was used to monitor the specific recognition of the epitope peptide in a bilayer milieu. Our data indicated that direct partitioning of the 4E10 antibody from the aqueous phase into membranes is driven by favorable electrostatic interactions between the surfaces of the membrane and the paratope. Although not strictly required for its biological function, electrostatic forces were also beneficial for binding to the membrane-anchored epitope peptide, and these favorable interactions correlated with the neutralizing potency of the 4E10 antibody. Collectively, our observations support the view that favorable, albeit unspecific, interactions between 4E10 and lipids play a central role in the neutralization mechanism by increasing potency of the antibody, while keeping its broad coverage.

RESULTS

Partitioning of 4E10 into membranes depends on anionic phospholipids—We first determined the partitioning of the 4E10 antibody into membranes using a vesicle flotation assay (FIG 1A). We note that in these experiments the amount of antibody incubated with vesicles was kept the same under all conditions tested, even though the intensity of the bands after Western-blotting slightly varied among the different samples. Results displayed in FIG 1B first reflected the different capacities of 10E8 and 4E10 antibodies for partitioning into virus-like (VL) membranes mimicking the viral envelope composition (22). The 10E8 antibody does not show lipid polyreactivity (3,23) or insertion into membranes devoid of peptide epitope (24) and, consequently, was used as a negative control for membrane binding in our assays. Thus, whereas

most of the 10E8 antibody was recovered from the high-density fractions (FIG 1B, first row), a major fraction of the input 4E10 antibody was recovered from the upper low-density fractions, i.e., co-floating with the VL vesicles (FIG 1B, second row). In search for a possible dependence of 4E10 binding-to-membranes on specific lipids, we subsequently established the contribution of each lipid present in the VL mixture to the process. Subtraction from the VL mixture of individual zwitterionic phospholipids (sphingomyelin (SM), or phosphatidylethanolamine (PE)), or cholesterol (Chol) one at a time, did not abolish membrane binding by 4E10 (FIG 1B, rows below 4E10 sample; lipid compositions displayed in Table 1). Control experiments indicated that removal of the bilayer-standard phospholipid phosphatidylcholine (PC) did not alter this antibody-vesicle binding pattern (not shown). In contrast, removal of the anionic phosphatidylserine (PS) from the composition of the vesicles prevented 4E10 to bind to the liposomes (FIG 1C, first row). To determine if binding was specific for PS, or resulted from unspecific electrostatic effects, we replaced PS with other anionic phospholipid species (i.e. PG, PI, PA or CL, rows below). The results convincingly showed that binding of 4E10 to liposomes was restored for all anionic phospholipids tested, indicating that membrane association did not require stereospecific recognition of a particular head-group (21).

Basic residues of the paratope promote partitioning of 4E10 into the membrane—The previous flotation experiments suggested that electrostatic interactions of 4E10 with anionic phospholipids promote its partitioning into membranes. Inspection of the surface of the paratope in contact with the membrane interface as inferred from the structure of Fab in complex with lipids (12), revealed a positively charged region (FIG 2A). We sought to elucidate the relevance of this charged patch for the electrostatic interaction of 4E10 with the membrane by separately mutating the basic residues Arg73_{HC} or Lys100_{HC} by a Glu residue (R73E and K100E mutants, respectively (FIG 2A)). We assumed that such substitutions, reversing the charge of the affected residues, would reduce the net positive charge at the base of the paratope, making the antibody less prone to interact electrostatically with the negatively charged membranes. The analysis

included a negative control designated as BS, in which residues Ser28 and Ser30 of the CDRH1 were mutated to Ala. These substitutions involved uncharged residues, and therefore did not presumably alter the surface charge of the paratope even if involving residues located in the lipid-binding sites (12).

FIG 2B illustrates the phenotypic traits resulting from the mutations with regard to membrane-binding. To obtain a more robust comparison, these assays employed membranes containing high levels of PS (PC:PS 1:1, mole ratio). As expected from a model dominated by electrostatic interactions, most of the input WT antibody associated with the vesicles. In contrast, the binding of R73E to the vesicles was reduced by approximately 50 %. The K100E mutant was not present in the floating fractions containing the vesicles, indicating an even weaker tendency to partition into membranes. The negative BS control reproduced rather well the behavior of the WT antibody. We arrived at similar conclusions using VL vesicles (see below).

Charge-reversing mutations interfere with the biological function of 4E10—We next examined the role of electrostatic forces in the biological function of the 4E10 antibody using the same collection of antibodies described immediately above (FIGs 3 and 4, and Table 1). First, ITC experiments were conducted to evaluate the effect of the mutations on the affinity for the epitope peptide MPER₍₆₆₄₋₆₉₀₎ (FIG 3A). We have shown in previous ITC experiments that this peptide mimics better the C-terminal MPER epitopes than peptides truncated at position 683 (24). The values of K_D determined from the binding isotherms were 4.6, 12.2 and 12.8 nM for the WT, BS and R73E antibodies, respectively (Table 1), i.e., within the same range of affinity previously determined for the 10E8 antibody (K_D , 9.6 nM (24)). A more significant reduction of affinity (\approx 20-fold) was observed in the case of the K100E mutant (K_D , 91 nM), although the variation in terms of free energy of binding was not so relevant (Table 1).

To assess the effect of the mutations on epitope-binding in a membrane context, flotation experiments were next carried out comparing the location of the Fab in the presence of bare VL vesicles, or VL vesicles decorated with the epitope peptide MPER₍₆₇₁₋₆₉₃₎ (FIG 3B). This peptide has

been shown to expose optimally the 4E10/10E8 epitope region on the surface of lipid vesicles (24,25). In the absence of peptide (left panel), the most conspicuous effect was observed for the K100eE mutant, which again did not appreciably associate with membranes in the VL system. As compared to WT or BS, a lower level of binding to LUVs was also evident for the R73E mutant. Incubation with VL-peptide complexes (right panel) resulted in the complete association of the WT and BS antibodies with vesicles. However, although a significant increase in binding to vesicles with respect to the bare vesicles was evident, association of R73E and K100eE variants with vesicles containing peptide was not complete.

The previous flotation results were obtained under conditions that promoted membrane partitioning (i.e., high lipid concentration (26)). To establish further differences in membrane affinities, binding to the vesicles as a function of the lipid concentration was monitored in dot-blot assays (FIG 3C). In this approach, measuring conditions were initially set up to reproduce the relative binding signals observed in flotation assays (i.e., to match signals of the Fabs recovered in the floating fractions). Titration of Fab-s with VL or VL-peptide complexes (left and right panels, respectively) confirmed the poor performance of the charge-reversing R73E and K100eE mutants for partitioning into membranes, as well as their lower affinity for vesicles containing the epitope peptide.

To establish a correlation between biological function, binding to membrane-embedded epitope, and membrane partitioning, the potency of the antibody and mutants was evaluated in neutralization assays (FIG 4A). The IC_{50} values determined for the mutants R73E and K100eE increased by approximately one order of magnitude with respect to WT and BS (FIG 4A and Table 1). Interestingly, the R73E and BS mutants bound to peptide by ITC with almost equal affinity, but their neutralization potencies were significantly different (Table 1). These data demonstrated that mutations reducing the electrostatic charge in the vicinity of the paratope have a negative impact not only in the binding to the epitope inserted in vesicles, but also in the biological function of the antibody. In contrast, the BS mutant reproduced for the most part the behavior of the WT Fab. Dot-blot assays indicated

that the reduced levels of activity of the mutants correlated well with lower binding of the mutant antibodies to pseudovirus immobilized on a solid substrate (FIG 4B). Overall, these results revealed a correlation between direct binding to immobilized pseudovirus (FIG 4B) and direct binding to immobilized vesicles containing the epitope peptide (FIG 3C, right panel).

Electrostatic interactions contribute to the efficient partitioning of 4E10 into membranes— The left panel of FIG 5A illustrates the difference in the conformation of the 4E10 CDRH3 loop in solution (PDB entry code 2FX7, gray) or embedded in a vesicle-like micellar structure made of dihexanoyl phosphatidic acid (PDB entry code 4XBG, white). Based on this observation, a movement of the CDRH3 loop was proposed to occur upon interaction of the antibody with the membrane (12). According to this model, the Trp100b_{HC} at the tip of the CDRH3 would relocate within the membrane interface to a position roughly equidistant from the headgroups and first methylene groups of the acyl chains of the lipids. Moreover, in a recent work we have shown that the polarity-sensitive NBD probe replacing Trp at the position 100b of the CDRH3 can be employed to monitor the insertion of the Fab 10E8 into the membrane (24). Here we have followed a similar strategy to characterize the association of 4E10 with membranes.

The right panels of FIG 5A display the changes in fluorescence that occur upon incubation of the NBD-Fab 4E10 with lipid vesicles. In the presence of VL vesicles, the fluorescence emission of the NBD attached to 4E10 shifted towards shorter wavelengths and its intensity increased. These two properties indicated that the dye (and therefore the apex of the CDRH3) its being transferred from a solvent-exposed environment to a more hydrophobic environment (27). The top panel in FIG 5A-right additionally illustrates the shift of emission to longer wavelengths when vesicles contained Rho-PE. This phenomenon occurred as a consequence of the resonance energy transfer between the NBD(donor)-Rhodamine(acceptor) pair (27). As displayed in the bottom panel, NBD fluorescence emission was also quenched by inclusion of 16:0-5 Doxyl PC in the lipid composition. The effects induced by these probes residing within the lipid bilayer demonstrated that NBD-Fab fluorescence

changes were caused by the antibody-membrane interaction. Such effects were further consistent with the interfacial location of the Trp100b_{HC} predicted by the model displayed in the left panel of FIG 5A.

We next analyzed the partitioning process quantitatively by monitoring the changes in NBD-Fab fluorescence that occur upon incubation of the Fab with increasing concentrations of VL LUVs (FIG 5B, left). Consistent with the restrained interaction deduced from the flotation assays (FIG 1C), the fluorescence of the NBD-Fab did not significantly change upon incubation with vesicles devoid of PS (FIG 5B, right). The titration values adjusted to Equation [1] (FIG 5C) from which a mole-fraction partition coefficient (K_x) of 0.6×10^6 was determined, a value that falls in the range of that observed for peripheral membrane proteins (28-30).

To evaluate the relative contribution of electrostatic interactions to the 4E10 partitioning process, titration experiments were conducted in a PC:PS model system (30,31). Thus, K_x values were calculated for vesicles containing different mol percentages of monovalent acidic PS (FIG 6). Association with vesicles increased with the PS content (FIGs 6A,B), following the pattern predicted from a favorable contribution of electrostatic interactions (30). The plot of the observed partitioning free energy (ΔG_{obs}) versus the surface potential (Ψ_0) calculated using Equations [2] and [3], respectively (32,33), yielded through extrapolation a ΔG_{obs} value of *ca.* -5 kcal mol⁻¹ for membranes lacking net charge (FIG 6C). This value indicates that, in the absence of anionic PS, a lipid concentration of *ca.* 15 mM would be required for 50 % of the Fab initially in solution be bound to membrane. In contrast, the value measured for pure PS vesicles was much more favorable ($\Delta G_{\text{obs}} = -8.8$ kcal mol⁻¹). A simple calculation using Equation [2] reveals that lipid diluted three orders of magnitude (i.e., 17.5 μ M) would be sufficient to attain a similar extent of Fab-membrane binding at room temperature.

Electrostatic interactions enhance epitope peptide binding by the 4E10 antibody—To infer the contribution of membrane partitioning to epitope recognition, we conducted experiments with PC:PS vesicles decorated with peptide epitope (FIG 7). Consistent with previous flotation results (FIG 4), the NBD emission spectra

obtained upon incubation with vesicles containing 25 or 50% of PS revealed a favorable contribution of both, anionic phospholipids and peptide epitope, to Fab partitioning (FIG 7A). Overall, the presence of peptide resulted in an increment of the partition constant, the effect being more pronounced with the highest proportion of PS (FIG 7B).

To study in more detail the combined effect of electrostatic interactions with the membrane surface and peptide recognition, we next performed time-course binding assays. FIG 7C displays the kinetic traces of the changes of fluorescence intensity that occurred upon injection of NBD-Fab (arrow) in a solution containing LUVs (left panel), or a solution containing LUV-peptide complexes (right panel). Addition of antibody to vesicles containing PS (25 or 50%) resulted in both cases in a sudden increase of fluorescence intensity followed by a signal plateau, consistent with a fast association to the membrane.

In contrast, upon addition of vesicles of the same composition containing the peptide, the sudden increase was followed by a second phase, in which the fluorescence signal increased gradually, leveling off at later times (right panel). Thus, whereas the fast phase of the NBD change can be explained by the spontaneous insertion into the membrane, the slower phase appears to be driven by specific peptide-recognition. Interestingly, the peptide-dependent slower phase observed for the 50 % mol PS LUVs (right panel, red line) was faster than that observed with 25 % mol PS. Thus, the PS appeared to have two effects. On the one hand, and as previously described, PS promoted higher levels of spontaneous incorporation. On the other hand, PS promoted faster recognition of the epitope peptide by the fraction of the Fab that had remained in solution.

Finally, to demonstrate peptide engagement under these conditions, we employed photo-cross-linking assays. To that end, the 4E10 Fab was modified with the UV-sensitive unnatural amino acid pBPA (34,35), which was genetically encoded at position Trp100b_{HC} of the antibody as previously described for the Fab 10E8 (24). Formation of covalent adducts were detected only when the lipid vesicles harbored the MPER₍₆₇₁₋₆₉₃₎ peptide, but not with vesicles devoid of peptide (FIG 7C, insets).

4E10 antibody pre-equilibrated on the membrane is competent for epitope engagement—Attachment of 4E10 molecules to virions without engagement to the epitope has been postulated as a mechanism favoring viral neutralization (36,37). This two-step model assumes that the fraction of 4E10 antibody pre-bound to the membrane engages with gp41 when viral fusion is activated. FIG 8 illustrates experiments to evaluate the capacity of the Fab for encountering and effectively engage the membrane-inserted epitope. To ensure that all Fab actually bound to membranes, we increased the lipid concentration in the assay, as well as the PS content in the vesicles. As explained in the diagram displayed in FIG 8A, under these conditions the subsequent process of peptide engagement can be scored by photo-cross-linking assays.

As expected, NBD-Fab addition to vesicles composed of 100% PS resulted in an abrupt and comparable increase of fluorescence in the presence and in the absence of epitope peptides (FIG 8B). The Fab-peptide complexes that could form under these conditions were subjected to UV light and the formation of adducts analyzed by SDS-PAGE and Western blot (FIG 8C). An additional band corresponding to cross-linked peptide (MPER₍₆₇₁₋₆₉₃₎) and Fab HC was observed in samples of *p*BPA-Fab incubated with liposome-peptide complexes (lane 1). A similar outcome was observed when *p*BPA-Fab and peptide were incubated in the absence of vesicles (lane 2). In contrast, the adduct band was not detected upon *p*BPA-Fab incubation with liposomes that contained a peptide with crucial residues for antibody binding Trp-672 and Phe-673 mutated to Ala (lane 3). This negative control was included to assure that adducts formed within vesicles came from specific peptide binding, and not from spontaneous cross-linking potentially promoted by the high densities of Fab and peptide attained at the membrane surface. Finally, a band corresponding to the Fab HC-peptide adduct was also observed when Fab was first pre-equilibrated on the membrane and peptide subsequently added to resulting liposome-Fab complexes (lane 4). These data clearly indicate that Fab pre-bound to membrane is competent in engagement with epitope.

DISCUSSION

The Env complex embodies the entry machinery of the HIV-1 and constitutes its main antigen (38,39). The gp41 MPER is highly conserved across the different HIV-1 strains and isolates, and is functionally involved in assisting the membrane fusion process that culminates with cell infection (40-42). Due to its high degree of sequence conservation and the key role played by this element in the viral cycle, the bNAbs 4E10 raised against the MPER exhibits an unusual neutralization breadth (5,43,44). It has been hypothesized that interactions with viral membrane lipids are required for the fulfillment of 4E10 biological function (9-12,17,36,45-49). However, a systematic and quantitative assessment of 4E10 partitioning into membranes was lacking. A detailed examination of this process is important for two reasons: i) to establish the lipid specificity range, which helps to evaluate the assumption that lipid auto-reactivity can prevent the production of 4E10-like antibodies through vaccination; and ii) to establish the contribution of membrane-assisted MPER engagement to the biological function of 4E10.

Relevance of spontaneous partitioning for the biological function of 4E10—Our data in FIGs 1-6 demonstrate that 4E10 partitioning into membranes is promoted by unspecific electrostatic interactions between the negatively charged membrane surface and the basic residues exposed on the paratope, and not by the stereospecific recognition of a particular phospholipid head-group (21). In this regard, 4E10 can be considered a peripheral membrane protein employing concerted electrostatic and hydrophobic forces to insert into membranes and engage its epitope (see for reviews: (29,50,51)). Herein we have examined the factors intervening in the electrostatically-driven partitioning of 4E10 in the membrane by employing two complementary approaches: i) by altering the surface charge of the Fab paratope via mutagenesis (FIGs 2-4); and ii) by modifying the density of monovalent anionic phospholipid in the membrane, particularly that of PS (FIGs 6-8).

As expected from the unspecific nature of electrostatic interactions, the mutation of basic residues as in R73E or K100E, clearly diminished the partitioning of the antibody into membranes. However, albeit less potent, these mutants were

still active in neutralization assays, an effect that correlated with weaker binding to immobilized PsVs or VL vesicles decorated with peptide. Thus, although comprising a modulatory factor for the amount of membrane-bound antibody, and hence, potency, partitioning driven by electrostatic interactions was not an absolute requirement for the neutralizing activity of the antibody. This key observation strongly suggests that the ability of the antibody to interact electrostatically with viral membranes needs an adaptation during the maturation pathway.

Our data employing vesicles with different surface charge densities also support the spontaneous interaction of 4E10 with negatively-charged membranes, (FIG 6), and that such interaction can contribute to the more efficient recognition of the membrane-bound epitope (FIGs 7 and 8). This is in contrast to the 10E8 interaction with membranes, which appears to depend on binding to peptide ligand anchored to the bilayer (24). However, the bNAb 10E8 displays higher potency than the antibody 4E10 and this phenomenon occurs without exhibiting binding to anionic phospholipid (FIG 1B and references (3,32)), or higher affinity for the epitope peptide MPER₍₆₆₄₋₆₉₀₎ by ITC (24). This important difference suggests that 4E10 and 10E8 follow different adaptive mechanisms to efficiently engage with the MPER helix at membrane interfaces, where the antibody exerts its viral neutralization activity.

Implications for the mechanism of neutralization by 4E10—Collectively, our data support the idea that direct interaction of 4E10 with the membrane is of high relevance for its neutralizing activity. FIG 9 illustrates three, non-exclusive mechanisms that have been previously proposed for the role of membrane interactions in the mechanism of 4E10 neutralization. We discuss the possible ways by which the peripheral membrane interactions described in this work may support these mechanisms:

I) Pre-concentration in the viral membrane (left): several authors have proposed a two-step mechanism for neutralization, in which 4E10 first attaches to the viral membrane (36,37). This reversible step would be required to ensure subsequent binding to target MPER epitope, which is transiently exposed after fusion activation. Pre-attachment implies first sufficient free energy for

driving spontaneous partitioning (a, in Fig. 9), and second, competence of the Fab pre-bound to membranes for subsequent specific recognition of the epitope ligand (b, in Fig. 9). Our quantitative measurements (FIGs 5-7) are consistent with partitioning constants in the range of those measured for peripheral membrane proteins (28-30). Moreover, by combining fluorescence spectroscopy and photo-cross-linking assays we were able to demonstrate the competence of antibody pre-bound to membrane for specific epitope binding (FIG 8). Thus, in principle, our *in vitro* data employing model systems are consistent with this mechanism.

II) Avidity effect (center): The surface of one virion particle only contains approximately ten Env complexes, and consequently the non-immunogenic lipid component of the envelope constitutes the main structural-functional element of the HIV particle that is accessible from the external milieu (52). The reduced accessibility to the epitope precludes bi-functional binding and has been thus regarded to as an evasion mechanism (6). Lipid polyreactivity may increase the avidity of IgG by endowing 4E10 with the capacity to directly interact with membranes (6,37). Our data support this notion, although we note that the association of 4E10 with the membrane is driven by unspecific electrostatic interactions.

III) Structural adaptation (right): the insertion of helical MPER epitope into the membrane interface imposes structural adaptations to the mechanism of recognition within the two-dimensional membrane milieu (17,49). It has been reported that PS becomes accessible at the external leaflet of membranes in mature virions (see for a discussion on this issue: (22)). Our data suggest that 4E10 takes the advantage of favorable electrostatic interactions with PS to enhance affinity for the membrane-bound epitope ligand (FIGs 3 and 7), most likely by providing an optimal orientation to the epitope-binding pocket relative to the membrane plane and sticking out MPER-helix.

In summary, our data support that electrostatic interactions with the negatively charged viral membrane surface contributes to enhance the affinity of 4E10 for the MPER helix and, hence, its potency. Assuming a constant lipid composition of virions across the different strains

and isolates of HIV-1, we speculate that this adaptation could have evolved through maturation without compromising the neutralization breadth of the antibody.

EXPERIMENTAL PROCEDURES

Materials—The peptides MPER₍₆₆₄₋₆₉₀₎:KKKK-DKWASLWNWFDITNWLWYIKLFIMIVG-KKKKK; MPER₍₆₇₁₋₆₉₃₎:KKK-NWFDITNWLWYIKLFIMIVGGLV-KK and MPER₍₆₇₁₋₆₉₃₎/W672A-F673A:KKK-NAADITNWLWYIKLFIMIVGGLV-KK were synthesized in C-terminal carboxamide form by solid-phase methods using Fmoc chemistry, purified by reverse phase HPLC, and characterized by matrix-assisted time-of-flight (MALDI-TOF) mass spectrometry (purity > 95 %). Peptides were routinely dissolved in dimethylsulfoxide (DMSO, spectroscopy grade) and their concentration determined by the bicinchoninic acid microassay (Pierce, Rockford, IL, USA). Experimental procedures described in (42,53) were followed for the production and purification of Fabs. Vector pEVOL, encoding a Tyr-tRNA synthetase suitable for the incorporation of photoreactive amino acid p-benzoylphenylalanine (pBPA), was a gift from Prof. P. G. Schultz (The Scripps Research Institute). pBPA was purchased from Bachem (Bubendorf, Switzerland) and 4-Chloro-7-Nitrobenz-2-Oxa-1,3-Diazole (NBD) from Thermofisher (Eugene, Oregon). All lipids including 1,2-dioleoyl-sn-glycerol-3-phosphoethanolamine-N-(lissamine rhodamine B sulfonyl) (Rho-PE) and 1-palmitoyl-2-stearoyl-(5-doxyl)-sn-glycero-3-phosphocholine (16:0-5 Doxyl PC) were purchased from Avanti Polar Lipids (Alabaster, Alabama).

Liposome flotation assays—Large unilamellar vesicles (LUV) were prepared following the extrusion method of Hope et al. (54). Phospholipids and cholesterol were mixed in chloroform and dried under a N₂ stream. Traces of organic solvent were removed by overnight vacuum pumping. Subsequently, the dried lipid films were dispersed in buffer, and subjected to 10 freeze-thaw cycles prior to extrusion 10 times through 2 stacked polycarbonate membranes with a nominal pore size of 100 nm (Nuclepore, Inc., Pleasanton, CA, USA). Phospholipid

concentration of liposome suspensions was determined by phosphate analysis. Chol content in vesicles was determined after extrusion by the cholesterol oxidase/peroxidase method (BioSystems, Barcelona, Spain) and found to be within the experimental error. Vesicle flotation experiments in sucrose gradients were subsequently performed following the method described by Yethon et al. (55). In brief, 100 μ l of a sample containing rhodamine-labeled liposomes and Fab (1.5 mM lipid, and 1.5 μ M Fab) was adjusted to a sucrose concentration of 1.4 M in a final volume of 300 μ l, and subsequently overlaid with 400 and 300 μ l-layers of 0.8 and 0.5 M sucrose, respectively. The gradient was centrifuged at 436,000 \times g for 3 h in a TLA 120.2 rotor (Beckman Coulter, Brea CA, USA). After centrifugation, four 250 μ l-fractions were collected as depicted in FIG 1A. The material adhered to the tubes was collected into a fifth fraction by washing with 250 μ l of hot (100 °C) 1 % (w/v) SDS. The different fractions were run on SDS-PAGE, and the presence of Fab probed by Western blotting using a sandwich comprising a goat (anti-human Fab) antibody (Sigma) and a mouse (anti-goat) antibody-HRP conjugate (Santa Cruz). Results displayed in Figures are representative of at least two replicates.

Isothermal titration calorimetry (ITC)—Titration experiments were performed with a VP-ITC microcalorimeter (MicroCal, Northampton, MA) at 25 °C. Prior to the experiment, proteins were dialyzed overnight at 4 °C against 10 mM sodium phosphate (pH 7.5), 150 mM NaCl, and 10 % glycerol. Samples containing protein and peptide solubilized in dialysis buffer were supplemented with 5 mM DPC and degassed immediately before each measurement. Fab 4E10 and mutant versions (3 μ M) was titrated with peptide (40 μ M). The volume of each injection was 10 μ L. Peptide dilution heat was subtracted for data analysis. The binding isotherms were fitted to a one-site binding model using the program O RIGIN 7.0. The fitting procedure yields the stoichiometry (n), the binding constant (K_D) and the enthalpy (ΔH°) of the binding reaction.

Cell entry inhibition—The cell entry inhibition assays were carried out as previously described (25,53,56). To run the experiments, HIV-

1 pseudoviruses were first produced by transfection of human kidney HEK293T cells with the full-length env clones HXB2 or JRCSF (kindly provided by Jamie K. Scott and Naveed Gulzar, Simon Fraser University, BC, Canada) using calcium phosphate. Cells were co-transfected with vectors pWXP-GFP and pCMV8.91, encoding a green fluorescent protein and an env-deficient HIV-1 genome, respectively (generously provided by Patricia Villace, CSIC, Madrid). After 24 h, the medium was replaced with Optimem-Glutamax II (Invitrogen Ltd, Paisley, UK) without serum. Three days after transfection, the pseudovirus particles were harvested, passed through 0.45 μ m pore sterile filters (Millex® HV, Millipore NV, Brussels, Belgium) and finally concentrated by ultracentrifugation in a sucrose gradient. Neutralization was determined using TZM-bl target cells (AIDS Research and Reference Reagent Program, Division of AIDS, NIAID, NIH, contributed by J. Kappes). Samples were set up in duplicate in 96-well plates, and incubated for 1.5 h at 37 °C with a 10-15 % tissue culture infectious dose of pseudovirus. After antibody-pseudovirus co-incubation, 11,000 target cells were added in the presence of 30 μ g/mL DEAE-dextran (Sigma-Aldrich, St-Louis, MO). Neutralization levels after 72 h were inferred from the reduction in the number of GFP-positive cells as determined by flow cytometry using a BD FACSCalibur Flow Cytometer (Becton Dickinson Immunocytometry Systems, Mountain View, CA).

Fab labeling with the NBD fluorescent probe and spectroscopic titration—Labeling with the polarity-sensitive NBD probe was performed as described (57,58). In brief, a cysteine-substituted Fab derivative (W100b_{HC}C) was first generated by site-directed mutagenesis and modified with a sulfhydryl-specific iodoacetamide derivative of NBD. Fluorescence emission spectra were recorded with the excitation wavelength fixed at 470 nm. An emission spectrum of a sample lacking the fluorophore was subtracted from the spectrum of the equivalent sample containing the fluorophore. Partitioning curves were computed from the fractional changes in emitted NBD-fluorescence when titrated with increasing lipid concentrations. The mole fraction partition coefficients, K_x , were

determined by fitting the experimental values to a hyperbolic function (26):

$$F/F_0 = 1 + \frac{[(F_{max}/F_0)-1] [L]}{K + [L]} \quad [1]$$

where [L] is the concentration of accessible lipid and K is the lipid concentration at which the bound peptide fraction is 0.5. Therefore, $K_x = [W]/K$ where [W] is the molar concentration of water. The observed free energy of water-membrane partitioning was subsequently calculated according to the following expression:

$$\Delta G_{obs} = -RT \ln K_x \quad [2]$$

For the estimation of the electrical potential at the membrane surface as a function of the PS content, the following equation was used:

$$\Psi_0 = [2kT/ze] \operatorname{arcsinh} [A\sigma/(c)^{1/2}] \quad [3]$$

where c is the number of ions per volume, and σ the surface charge density (33). To calculate the latter parameter a surface area per phospholipid of 69.5 \AA^2 was considered, and net charges of 0 and -1 assigned to PC and PS, respectively (59).

Fab labeling with photo-activable amino acid—For the photo-cross-linking experiments, an amber codon specific for an engineered tRNA that translates the unnatural amino acid, *p*BPA, was encoded in the DNA sequence of the heavy chain of the 4E10 Fab. Procedures to express a 4E10 Fab mutant bearing *p*BPA instead of Trp at position 100b_{HC} were adapted from previous reports (34,35). Synthesis of Fab and the engineered tRNA was induced with 0.4 mM isopropyl-D-thiogalactopyranoside (IPTG) and 4 % (w/v) arabinose, respectively, in LB medium supplemented with 0.2 mg/L *p*BPA. For the photo-cross-linking experiment, samples containing Fab bearing the Trp100b_{HC} x *p*BPA substitution at 1.5 μ M and peptides at 10 μ M were irradiated with UV light at 365 nm for 20 min at 4 °C using a UVP B-100AP lamp.

Acknowledgements: This work was supported by the NIH and the Basque Government (grants AI097051 and IT838-13 to J.L.N.). Work in the laboratory of K.T. was supported by JSPS KAKENHI-A grants 25249115 and 16H02420 (to K.T.), by the Platform for Drug Discovery, Informatics and Structural Life Science from the Ministry of Education, Culture, Sports, Science and Technology of Japan and by a JSPS KAKENHI-C grant 15K06962 (to J.M.M.C.). E.R. was recipient of a predoctoral fellowship from the Basque Government. We thank Dr. Apellaniz for helpful discussions.

Conflict of interest: The authors declare that they have no conflicts of interests with the contents of this article.

Author contributions: E.R., J.M.M.C., K.T. and J.L.N. conceived and designed the experiments; E.R. produced Fabs and performed biophysical and biochemical characterizations with assistance of S.I. and M.G.-M.; E.R., J.M.M.C. and J.L.N. wrote the paper with input from K.T., and all authors reviewed it.

References

1. Zwick, M. B., Labrijn, A. F., Wang, M., Spenlehauer, C., Saphire, E. O., Binley, J. M., Moore, J. P., Stiegler, G., Katinger, H., Burton, D. R., and Parren, P. W. (2001) Broadly neutralizing antibodies targeted to the membrane-proximal external region of human immunodeficiency virus type 1 glycoprotein gp41. *J Virol* **75**, 10892-10905
2. Binley, J. M., Wrin, T., Korber, B., Zwick, M. B., Wang, M., Chappey, C., Stiegler, G., Kunert, R., Zolla-Pazner, S., Katinger, H., Petropoulos, C. J., and Burton, D. R. (2004) Comprehensive cross-clade neutralization analysis of a panel of anti-human immunodeficiency virus type 1 monoclonal antibodies. *J Virol* **78**, 13232-13252
3. Huang, J., Ofek, G., Laub, L., Louder, M. K., Doria-Rose, N. A., Longo, N. S., Imamichi, H., Bailer, R. T., Chakrabarti, B., Sharma, S. K., Alam, S. M., Wang, T., Yang, Y., Zhang, B., Migueles, S. A., Wyatt, R., Haynes, B. F., Kwong, P. D., Mascola, J. R., and Connors, M. (2012) Broad and potent neutralization of HIV-1 by a gp41-specific human antibody. *Nature* **491**, 406-412
4. Jacob, R. A., Moyo, T., Schomaker, M., Abrahams, F., Grau Pujol, B., and Dorfman, J. R. (2015) Anti-V3/Glycan and Anti-MPER Neutralizing Antibodies, but Not Anti-V2/Glycan Site Antibodies, Are Strongly Associated with Greater Anti-HIV-1 Neutralization Breadth and Potency. *J Virol* **89**, 5264-5275
5. Montero, M., van Houten, N. E., Wang, X., and Scott, J. K. (2008) The membrane-proximal external region of the human immunodeficiency virus type 1 envelope: dominant site of antibody neutralization and target for vaccine design. *Microbiol Mol Biol Rev* **72**, 54-84, table of contents
6. Klein, F., Mouquet, H., Dosenovic, P., Scheid, J. F., Scharf, L., and Nussenzweig, M. C. (2013) Antibodies in HIV-1 vaccine development and therapy. *Science* **341**, 1199-1204
7. Kim, A. S., Leaman, D. P., and Zwick, M. B. (2014) Antibody to gp41 MPER alters functional properties of HIV-1 Env without complete neutralization. *PLoS Pathog* **10**, e1004271
8. Sanchez-Martinez, S., Lorizate, M., Hermann, K., Kunert, R., Basanez, G., and Nieva, J. L. (2006) Specific phospholipid recognition by human immunodeficiency virus type-1 neutralizing anti-gp41 2F5 antibody. *FEBS Lett* **580**, 2395-2399
9. Matyas, G. R., Beck, Z., Karasavvas, N., and Alving, C. R. (2009) Lipid binding properties of 4E10, 2F5, and WR304 monoclonal antibodies that neutralize HIV-1. *Biochim Biophys Acta* **1788**, 660-665
10. Finton, K. A., Larimore, K., Larman, H. B., Friend, D., Correnti, C., Rupert, P. B., Elledge, S. J., Greenberg, P. D., and Strong, R. K. (2013) Autoreactivity and exceptional CDR plasticity (but not unusual polyspecificity) hinder elicitation of the anti-HIV antibody 4E10. *PLoS Pathog* **9**, e1003639
11. Chen, J., Frey, G., Peng, H., Rits-Volloch, S., Garrity, J., Seaman, M. S., and Chen, B. (2014) Mechanism of HIV-1 neutralization by antibodies targeting a membrane-proximal region of gp41. *J Virol* **88**, 1249-1258
12. Irimia, A., Sarkar, A., Stanfield, R. L., and Wilson, I. A. (2016) Crystallographic Identification of Lipid as an Integral Component of the Epitope of HIV Broadly Neutralizing Antibody 4E10. *Immunity* **44**, 21-31
13. Alving, C. R. (2008) 4E10 and 2F5 monoclonal antibodies: binding specificities to phospholipids, tolerance, and clinical safety issues. *Aids* **22**, 649-651
14. Haynes, B. F., Fleming, J., St Clair, E. W., Katinger, H., Stiegler, G., Kunert, R., Robinson, J., Searce, R. M., Plonk, K., Staats, H. F., Ortel, T. L., Liao, H. X., and Alam, S. M. (2005) Cardiolipin polyspecific autoreactivity in two broadly neutralizing HIV-1 antibodies. *Science* **308**, 1906-1908

15. Doyle-Cooper, C., Hudson, K. E., Cooper, A. B., Ota, T., Skog, P., Dawson, P. E., Zwick, M. B., Schief, W. R., Burton, D. R., and Nemazee, D. (2013) Immune tolerance negatively regulates B cells in knock-in mice expressing broadly neutralizing HIV antibody 4E10. *J Immunol* **191**, 3186-3191
16. Verkoczy, L., Kelsoe, G., and Haynes, B. F. (2014) HIV-1 envelope gp41 broadly neutralizing antibodies: hurdles for vaccine development. *PLoS Pathog* **10**, e1004073
17. Sanchez-Martinez, S., Lorizate, M., Katinger, H., Kunert, R., and Nieva, J. L. (2006) Membrane association and epitope recognition by HIV-1 neutralizing anti-gp41 2F5 and 4E10 antibodies. *AIDS Res Hum Retroviruses* **22**, 998-1006
18. Rujas, E., Gulzar, N., Morante, K., Tsumoto, K., Scott, J. K., Nieva, J. L., and Caaveiro, J. M. (2015) Structural and Thermodynamic Basis of Epitope Binding by Neutralizing and Nonneutralizing Forms of the Anti-HIV-1 Antibody 4E10. *J Virol* **89**, 11975-11989
19. Rujas, E., Gulzar, N., Morante, K., Tsumoto, K., Scott, J. K., Nieva, J. L., and Caaveiro, J. M. (2016) Reply to "The Broadly Neutralizing, Anti-HIV Antibody 4E10: an Open and Shut Case?". *J Virol* **90**, 3276-3277
20. Bird, G. H., Irimia, A., Ofek, G., Kwong, P. D., Wilson, I. A., and Walensky, L. D. (2014) Stapled HIV-1 peptides recapitulate antigenic structures and engage broadly neutralizing antibodies. *Nat Struct Mol Biol* **21**, 1058-1067
21. Lemmon, M. A. (2008) Membrane recognition by phospholipid-binding domains. *Nature reviews. Molecular cell biology* **9**, 99-111
22. Huarte, N., Carravilla, P., Cruz, A., Lorizate, M., Nieto-Garai, J. A., Krausslich, H. G., Perez-Gil, J., Requejo-Isidro, J., and Nieva, J. L. (2016) Functional organization of the HIV lipid envelope. *Scientific reports* **6**, 34190
23. Kwon, Y. D., Georgiev, I. S., Ofek, G., Zhang, B., Asokan, M., Bailer, R. T., Bao, A., Caruso, W., Chen, X., Choe, M., Druz, A., Ko, S. Y., Louder, M. K., McKee, K., O'Dell, S., Pegu, A., Rudicell, R. S., Shi, W., Wang, K., Yang, Y., Alger, M., Bender, M. F., Carlton, K., Cooper, J. W., Blinn, J., Eudailey, J., Lloyd, K., Parks, R., Alam, S. M., Haynes, B. F., Padte, N. N., Yu, J., Ho, D. D., Huang, J., Connors, M., Schwartz, R. M., Mascola, J. R., and Kwong, P. D. (2016) Optimization of the Solubility of HIV-1-Neutralizing Antibody 10E8 through Somatic Variation and Structure-Based Design. *J Virol* **90**, 5899-5914
24. Rujas, E., Caaveiro, J. M., Partida-Hanon, A., Gulzar, N., Morante, K., Apellaniz, B., Garcia-Porras, M., Bruix, M., Tsumoto, K., Scott, J. K., Jimenez, M. A., and Nieva, J. L. (2016) Structural basis for broad neutralization of HIV-1 through the molecular recognition of 10E8 helical epitope at the membrane interface. *Scientific reports* **6**, 38177
25. Apellaniz, B., Rujas, E., Serrano, S., Morante, K., Tsumoto, K., Caaveiro, J. M., Jimenez, M. A., and Nieva, J. L. (2015) The Atomic Structure of the HIV-1 gp41 Transmembrane Domain and Its Connection to the Immunogenic Membrane-proximal External Region. *J Biol Chem* **290**, 12999-13015
26. White, S. H., Wimley, W. C., Ladokhin, A. S., and Hristova, K. (1998) Protein folding in membranes: Determining energetics of peptide-bilayer interactions. in *Methods in Enzymology*, Academic Press. pp 62-87
27. Lakowicz, J. R. (2006) *Principles of Fluorescence Spectroscopy*, 3 ed., Springer US
28. Nomikos, M., Mulgrew-Nesbitt, A., Pallavi, P., Mihalyne, G., Zaitseva, I., Swann, K., Lai, F. A., Murray, D., and McLaughlin, S. (2007) Binding of phosphoinositide-specific phospholipase C-zeta (PLC-zeta) to phospholipid membranes: potential role of an unstructured cluster of basic residues. *J Biol Chem* **282**, 16644-16653

29. Mulgrew-Nesbitt, A., Diraviyam, K., Wang, J., Singh, S., Murray, P., Li, Z., Rogers, L., Mirkovic, N., and Murray, D. (2006) The role of electrostatics in protein-membrane interactions. *Biochim Biophys Acta* **1761**, 812-826
30. Arbuzova, A., Wang, J., Murray, D., Jacob, J., Cafiso, D. S., and McLaughlin, S. (1997) Kinetics of interaction of the myristoylated alanine-rich C kinase substrate, membranes, and calmodulin. *J Biol Chem* **272**, 27167-27177
31. Arbuzova, A., Wang, L., Wang, J., Hangyas-Mihalyne, G., Murray, D., Honig, B., and McLaughlin, S. (2000) Membrane binding of peptides containing both basic and aromatic residues. Experimental studies with peptides corresponding to the scaffolding region of caveolin and the effector region of MARCKS. *Biochemistry* **39**, 10330-10339
32. White, S. H., and Wimley, W. C. (1999) Membrane protein folding and stability: physical principles. *Annu Rev Biophys Biomol Struct* **28**, 319-365
33. McLaughlin, S. (1989) The electrostatic properties of membranes. *Annual review of biophysics and biophysical chemistry* **18**, 113-136
34. Young, T. S., Ahmad, I., Yin, J. A., and Schultz, P. G. (2010) An enhanced system for unnatural amino acid mutagenesis in E. coli. *J Mol Biol* **395**, 361-374
35. Abe, R., Caaveiro, J. M., Kozuka-Hata, H., Oyama, M., and Tsumoto, K. (2012) Mapping ultra-weak protein-protein interactions between heme transporters of Staphylococcus aureus. *J Biol Chem* **287**, 16477-16487
36. Alam, S. M., Morelli, M., Dennison, S. M., Liao, H. X., Zhang, R., Xia, S. M., Rits-Volloch, S., Sun, L., Harrison, S. C., Haynes, B. F., and Chen, B. (2009) Role of HIV membrane in neutralization by two broadly neutralizing antibodies. *Proc Natl Acad Sci U S A* **106**, 20234-20239
37. Haynes, B. F., Nicely, N. I., and Alam, S. M. (2010) HIV-1 autoreactive antibodies: are they good or bad for HIV-1 prevention? *Nat Struct Mol Biol* **17**, 543-545
38. Wyatt, R., and Sodroski, J. (1998) The HIV-1 envelope glycoproteins: fusogens, antigens, and immunogens. *Science* **280**, 1884-1888
39. Karlsson Hedestam, G. B., Fouchier, R. A., Phogat, S., Burton, D. R., Sodroski, J., and Wyatt, R. T. (2008) The challenges of eliciting neutralizing antibodies to HIV-1 and to influenza virus. *Nat Rev Microbiol* **6**, 143-155
40. Salzwedel, K., West, J. T., and Hunter, E. (1999) A conserved tryptophan-rich motif in the membrane-proximal region of the human immunodeficiency virus type 1 gp41 ectodomain is important for Env-mediated fusion and virus infectivity. *J Virol* **73**, 2469-2480
41. Saez-Cirion, A., Nir, S., Lorizate, M., Agirre, A., Cruz, A., Perez-Gil, J., and Nieva, J. L. (2002) Sphingomyelin and cholesterol promote HIV-1 gp41 pretransmembrane sequence surface aggregation and membrane restructuring. *J Biol Chem* **277**, 21776-21785
42. Apellaniz, B., Rujas, E., Carravilla, P., Requejo-Isidro, J., Huarte, N., Domene, C., and Nieva, J. L. (2014) Cholesterol-Dependent Membrane Fusion Induced by the gp41 Membrane-Proximal External Region-Transmembrane Domain Connection Suggests a Mechanism for Broad HIV-1 Neutralization. *J Virol* **88**, 13367-13377
43. Zwick, M. B. (2005) The membrane-proximal external region of HIV-1 gp41: a vaccine target worth exploring. *Aids* **19**, 1725-1737

44. Kwong, P. D., and Mascola, J. R. (2012) Human antibodies that neutralize HIV-1: identification, structures, and B cell ontogenies. *Immunity* **37**, 412-425
45. Cardoso, R. M., Zwick, M. B., Stanfield, R. L., Kunert, R., Binley, J. M., Katinger, H., Burton, D. R., and Wilson, I. A. (2005) Broadly neutralizing anti-HIV antibody 4E10 recognizes a helical conformation of a highly conserved fusion-associated motif in gp41. *Immunity* **22**, 163-173
46. Huarte, N., Lorizate, M., Maeso, R., Kunert, R., Arranz, R., Valpuesta, J. M., and Nieva, J. L. (2008) The broadly neutralizing anti-human immunodeficiency virus type 1 4E10 monoclonal antibody is better adapted to membrane-bound epitope recognition and blocking than 2F5. *J Virol* **82**, 8986-8996
47. Sun, Z. Y., Oh, K. J., Kim, M., Yu, J., Brusic, V., Song, L., Qiao, Z., Wang, J. H., Wagner, G., and Reinherz, E. L. (2008) HIV-1 broadly neutralizing antibody extracts its epitope from a kinked gp41 ectodomain region on the viral membrane. *Immunity* **28**, 52-63
48. Dennison, S. M., Stewart, S. M., Stempel, K. C., Liao, H. X., Haynes, B. F., and Alam, S. M. (2009) Stable docking of neutralizing human immunodeficiency virus type 1 gp41 membrane-proximal external region monoclonal antibodies 2F5 and 4E10 is dependent on the membrane immersion depth of their epitope regions. *J Virol* **83**, 10211-10223
49. Scherer, E. M., Leaman, D. P., Zwick, M. B., McMichael, A. J., and Burton, D. R. (2010) Aromatic residues at the edge of the antibody combining site facilitate viral glycoprotein recognition through membrane interactions. *Proc Natl Acad Sci U S A* **107**, 1529-1534
50. McLaughlin, S., and Aderem, A. (1995) The myristoyl-electrostatic switch: a modulator of reversible protein-membrane interactions. *Trends Biochem Sci* **20**, 272-276
51. Gelb, M. H., Cho, W., and Wilton, D. C. (1999) Interfacial binding of secreted phospholipases A(2): more than electrostatics and a major role for tryptophan. *Curr Opin Struct Biol* **9**, 428-432
52. Zhu, P., Liu, J., Bess, J., Jr., Chertova, E., Lifson, J. D., Grise, H., Ofek, G. A., Taylor, K. A., and Roux, K. H. (2006) Distribution and three-dimensional structure of AIDS virus envelope spikes. *Nature* **441**, 847-852
53. Julien, J. P., Huarte, N., Maeso, R., Taneva, S. G., Cunningham, A., Nieva, J. L., and Pai, E. F. (2010) Ablation of the complementarity-determining region H3 apex of the anti-HIV-1 broadly neutralizing antibody 2F5 abrogates neutralizing capacity without affecting core epitope binding. *J Virol* **84**, 4136-4147
54. Hope, M. J., Bally, M. B., Webb, G., and Cullis, P. R. (1985) Production of large unilamellar vesicles by a rapid extrusion procedure. Characterization of size distribution, trapped volume and ability to maintain a membrane potential. *Biochim. Biophys. Acta* **812**, 55-65
55. Yethon, J. A., Epand, R. F., Leber, B., Epand, R. M., and Andrews, D. W. (2003) Interaction with a membrane surface triggers a reversible conformational change in Bax normally associated with induction of apoptosis. *J Biol Chem* **278**, 48935-48941
56. Serrano, S., Araujo, A., Apellaniz, B., Bryson, S., Carravilla, P., de la Arada, I., Huarte, N., Rujas, E., Pai, E. F., Arrondo, J. L., Domene, C., Jimenez, M. A., and Nieva, J. L. (2014) Structure and immunogenicity of a peptide vaccine, including the complete HIV-1 gp41 2F5 epitope: implications for antibody recognition mechanism and immunogen design. *J Biol Chem* **289**, 6565-6580
57. Shepard, L. A., Heuck, A. P., Hamman, B. D., Rossjohn, J., Parker, M. W., Ryan, K. R., Johnson, A. E., and Tweten, R. K. (1998) Identification of a membrane-spanning domain of the thiol-activated pore-forming toxin *Clostridium perfringens* perfringolysin O: an alpha-helical to beta-sheet transition identified by fluorescence spectroscopy. *Biochemistry* **37**, 14563-14574

- 58. Heuck, A. P., Hotze, E. M., Tweten, R. K., and Johnson, A. E. (2000) Mechanism of membrane insertion of a multimeric beta-barrel protein: perfringolysin O creates a pore using ordered and coupled conformational changes. *Molecular cell* **6**, 1233-1242
- 59. Rand, R. P., and Parsegian, V. A. (1989) Hydration forces between phospholipid bilayers. *Biochim Biophys Acta* **988**, 351-376

FOOTNOTES

¹The abbreviations used are: bNAb, broadly neutralizing antibody; CDR, complementarity determining region; MPER, membrane-proximal external region; NBD, 4-Chloro-7-Nitrobenz-2-Oxa-1,3-Diazole; *p*BPA, *p*-benzoylphenylalanine; PS, phosphatidylserine; VL, virus-like.

TABLES

Table 1. Composition of Virus-like (VL) lipid mixtures used in this work^a

| | PC | CHOL | SM | PE | PS |
|-----------------------------|----|------|----|----|----|
| VL | 14 | 46 | 17 | 16 | 7 |
| w/o SM^b | 31 | 46 | - | 16 | 7 |
| w/o PE^b | 30 | 46 | 17 | - | 7 |
| w/o Chol^c | 27 | - | 30 | 29 | 14 |
| w/o PS^b | 21 | 46 | 17 | 16 | - |

^a Mole percentage of lipid

^b Contribution of phospholipids added to PC

^c Contribution of Chol distributed proportionally among the other lipids

Table 2. Thermodynamic parameters of binding^a of Fab 4E10 mutants to the MPER₍₆₆₄₋₆₉₀₎ peptide and their neutralization potencies.

| <i>Antibody</i> (4E10) | <i>K_D</i> (nM) ^b | <i>ΔG°</i> (kcal mol ⁻¹) | <i>ΔH°</i> (kcal mol ⁻¹) | <i>-TΔS°</i> (kcal mol ⁻¹) ^a | <i>c</i> ^b | <i>HXB2-IC₅₀</i> (μg/mL) ^d | <i>JRCSE-IC₅₀</i> (μg/mL) ^d |
|---------------------------|---|---|---|--|-----------------------|---|--|
| 4E10_WT | 4.6 ± 1.5 | -11.4 ± 0.2 | -15.1 ± 0.2 | 3.7 | 1.0 ± 0.1 | 0.21 ± 0.02 | 1.26 ± 0.09 |
| BS | 12.2 ± 2.5 | -10.8 ± 0.1 | -11.7 ± 0.1 | 0.9 | 1.3 ± 0.1 | 0.38 ± 0.03 | 1.59 ± 0.27 |
| R73E | 12.8 ± 3.5 | -10.8 ± 0.1 | -14.7 ± 0.2 | 3.9 | 1.1 ± 0.1 | 5.3 ± 0.4 | 13.2 ± 3.5 |
| K100eE | 91 ± 14 | -9.6 ± 0.2 | -10.4 ± 0.2 | 0.7 | 1.4 ± 0.1 | 3.3 ± 0.2 | 12.7 ± 4.0 |

^a Temperature was 298 K.

^b Values are determined errors ± ??? as inferred from ??? Jose

^c *n* refers to the molar ratio peptide/protein.

^d Values determined ??? Edurne

FIGURE LEGENDS

FIG 1. Partitioning of the anti-MPER 4E10 Fab into membranes. A) 4E10 membrane partitioning detected in a sucrose gradient. Lipid vesicles incubated with the Fab were subject to centrifugation. The sample was divided into four different fractions based on their different densities. An additional fraction employing SDS was collected, representing the material attached to the surface of the tube. The location of the liposomes in the third and fourth fractions (i.e., floating fractions) was verified from the Rho-PE emission (bottom panels). The presence of Fab was probed by Western-blot. B) Effect of the constituent lipids of the VL mixture on the process (lipid compositions are given in Table 1). 10E8 antibody was used as negative control (first row). C) Effect of removing PS from the composition (first row) and recovery of membrane binding by its replacement with other anionic phospholipids; PG, PI, PA or CL. The band corresponding to the Fabs co-migrated in the gels with the 25 kDa molecular weight marker (indicated by the ticks, only in the first rows in panel B and C).

FIG 2. Design of 4E10 mutants with exposed basic residues of the paratope. A) Effect of R73E and K100eE substitutions on the surface charge of the paratope. B) Membrane partitioning as measured by flotation assays using vesicles containing 50 mol % of anionic lipid (PS) and PC. BS stands for a negative control with a double Ser-to-Ala substitution at positions 28 and 30 of the heavy chain.

FIG 3. Functional characterization of 4E10 mutants: binding to epitope peptide. A) Binding isotherms of the MPER₍₆₆₄₋₆₉₀₎ epitope peptide to Fab 4E10 examined by ITC. The upper panel indicates the heat released upon consecutive injections of 10 μ L of peptide solution (40 μ M) into Fab (3 μ M) in the calorimeter cell, and the lower panel the integrated heats (symbols) and non-linear least-squares fit (solid line) to the data using a one site binding model with the program ORIGIN 7.0. The thermodynamic parameters of binding are displayed in Table 1. B) Flotation experiments in the presence of VL LUVs (left) or VL LUVs containing MPER₍₆₇₁₋₆₉₃₎ peptide (right). C) Recognition of VL LUVs (left) or VL LUVs containing MPER₍₆₇₁₋₆₉₃₎ peptide (right) as determined by dot blot analysis. 2-fold serial dilutions of 500 μ M LUVs and 10 μ M peptide was spotted on the filters

FIG 4. Functional characterization of 4E10 mutants: biological activity. A) PsV neutralization potency of the different mutants. Means of 6 measurements \pm SD are represented in the plots. The experimental points were fitted to a saturation curve. B) JRCSF PsV recognition as determined by dot blot analysis. Decreasing amounts of PsV (from left to right) were spotted onto nitrocellulose membranes and probed with 4E10 Fab WT and its mutants.

FIG 5. Binding of 4E10 to VL LUVs monitored by changes in NBD fluorescence. A) Left: repositioning of CDRH3 loop Trp100b_{HC} residue upon 4E10 interaction with membranes. The loops were modeled according to crystal structures with PDB entries 2FX7 and 4XBG (gray and white, respectively). A second phospholipid molecule was aligned with that bound in 4XBG crystal. Right: changes in fluorescence that occur upon incubation of the Fab 4E10 labeled with NBD at position 100b_{HC} with lipid vesicles. Top: solid lines correspond to NBD-4E10 incubated in solution (black) or in presence of 100 or 200 μ M VL liposomes (red and blue respectively). Dotted lines correspond to incubations with VL liposomes containing 0.25 mol % of Rho-PE. Bottom: NBD-Fab was incubated with VL LUVs or VL LUVs containing 10 mol % 16:0-5 Doxyl PC (red-solid and red-dotted, respectively). B) Titration of NBD-labeled Fab with increasing concentrations of VL liposomes as indicated in the panels. C) Plot of the fraction of Fab bound as a function of the concentration of lipid accessible (half the total lipid concentration). The molar fraction partition coefficient, K_x , was calculated from the best fit of Equation [1] to the data (curve). Each symbol on the plot represents an average of three independent experiments (\pm S.D. if larger than symbol). 150 nM of NBD-Fab was used in these experiments.

FIG 6. Effect of anionic phospholipid density on 4E10 binding to LUVs. A) Changes of NBD-4E10 fluorescence in the presence of increasing concentrations PS LUVs as indicated in the panel. B) Titration of NBD-labeled Fab with vesicles containing different mol percentages of PC:PS as follows: 90:10 (gray); 75:25 (magenta); 50:50 (green); 25:75 (blue); 0:100 (red). The molar fraction partition coefficients, K_x , were calculated from the best fit of Equation [1] to the data (curves). Each symbol on the plot represents the average (\pm S.D.) of three independent experiments as the one displayed in the previous panel. C) Plot of the free energy of partitioning versus the membrane-surface potential in the previous lipid vesicles, estimated according to Equations [2] and [3], respectively. Conditions otherwise as in previous FIG 5.

FIG 7. Effect of electrostatic interactions on epitope recognition at the membrane surface. A) Changes of NBD-4E10 fluorescence emission spectra in the presence of increasing concentrations of vesicles as indicated in the panel, were measured in the absence (dotted lines) or in the presence of 1.7 μ M of MPER₍₆₇₁₋₆₉₃₎ peptide inserted in the membrane (solid lines). B) Effect of PS on Fab 4E10 partitioning into vesicles with and without MPER₍₆₇₁₋₆₉₃₎ peptide inserted in the membrane. NBD-Fab was titrated with PC:PS LUVs as indicated. Each data point corresponds to the average of three titrations (\pm SD) as the ones displayed in the previous panel. C) Kinetics of incorporation of NBD-Fab into bare vesicles containing 25 or 50 % of PS (left panel) or into the same vesicles decorated with 1.7 μ M MPER₍₆₇₁₋₆₉₃₎ peptide (right panel). The arrow indicates NBD-Fab addition. Fab-peptide interaction was assayed by photo-cross-linking using Fab-*p*BPA and 25 % PS vesicles. The presence of an adduct band confirmed Fab-peptide interaction in peptide-containing vesicles (insets). Lipid concentration was 100 μ M. Results representative of two replicas are presented.

FIG 8. Epitope recognition by 4E10 antibody bound to membrane A) Schematic representation of the assay showing partitioning of the Fab into the membrane (top) and its movement through the surface until the encounter and efficient engagement with epitope peptide (bottom). This latter event can be scored by photo-cross-linking. B) Kinetics of NBD-Fab incorporation into pure PS vesicles in the presence (red line) or absence of MPER₍₆₇₁₋₆₉₃₎ peptide (black solid line). Lipid and peptide concentrations were 250 and 1.7 μ M, respectively. The dotted line corresponds to the signal of the NBD-Fab in solution. The arrow indicates the NBD-Fab addition time. C) Photo-cross-linking experiments: (1) *p*BPA-Fab4E10 was added to PS vesicles decorated with MPER₍₆₇₁₋₆₉₃₎ (red kinetic trace in previous panel); (2) *p*BPA-Fab4E10 and MPER₍₆₇₁₋₆₉₃₎ peptide were incubated in the absence of PS vesicles; (3) *p*BPA-Fab4E10 was incubated with vesicles that contained the MPER₍₆₇₁₋₆₉₃₎/W672A-F673A peptide; (4) *p*BPA-Fab4E10 was first incorporated into vesicles (see black kinetic trace in previous panel) and after 1 min MPER₍₆₇₁₋₆₉₃₎ was added. Protein bands were detected by Coomassie staining or Western blot (top and bottom panels, respectively). Lipid and peptide concentrations as in the previous panel. Results representative of two replicas are presented in panels B and C.

FIG 9. Summary of mechanisms to explain the involvement of electrostatic interactions in MPER helix engagement and ensuing neutralization. See Discussion for details.

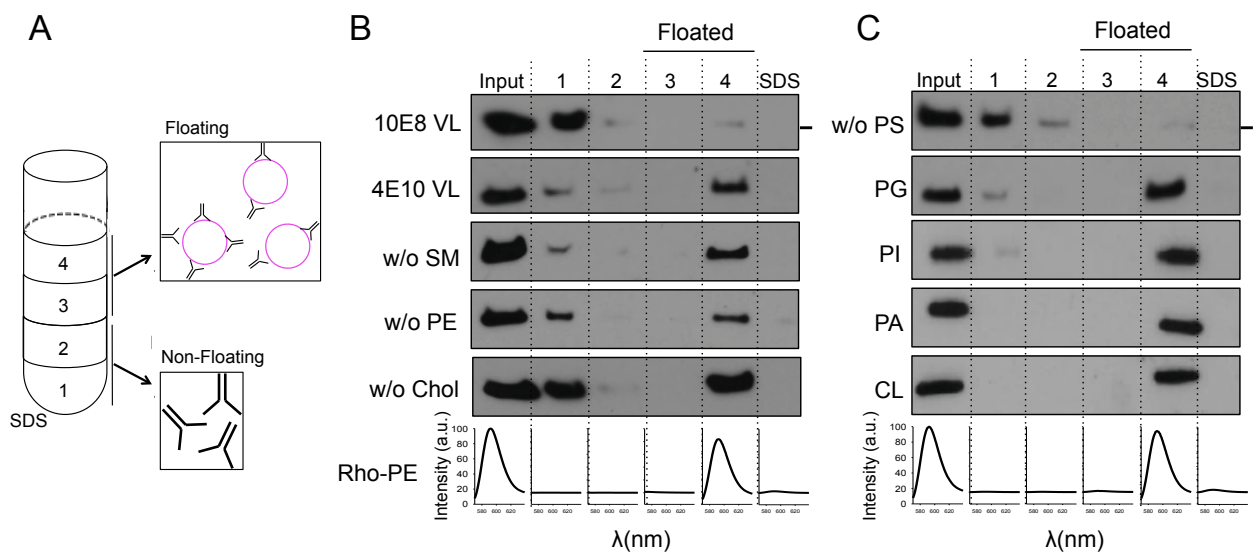


Figure 1

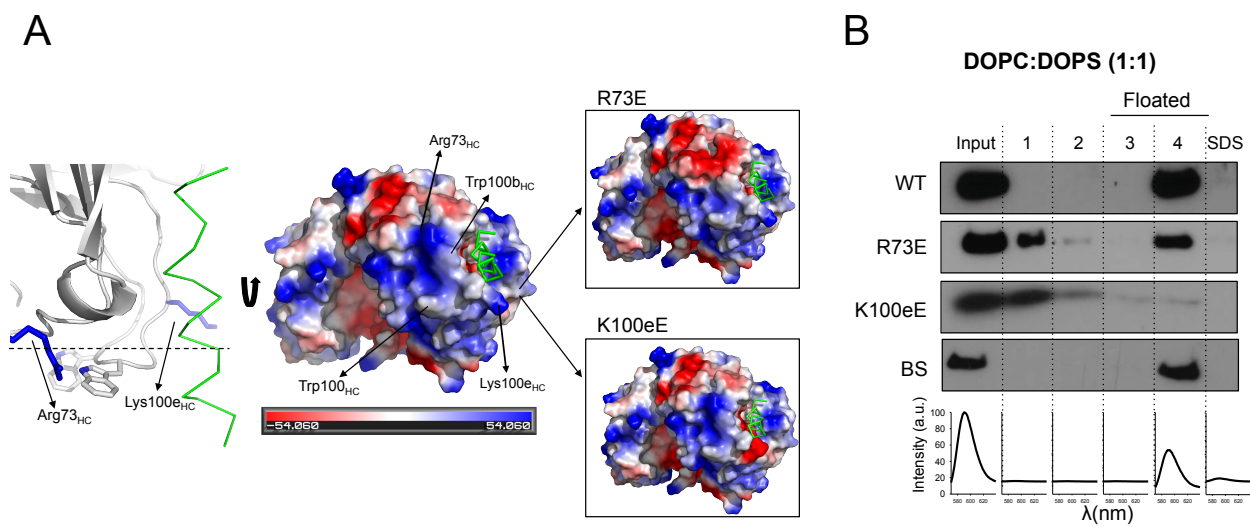


Figure 2

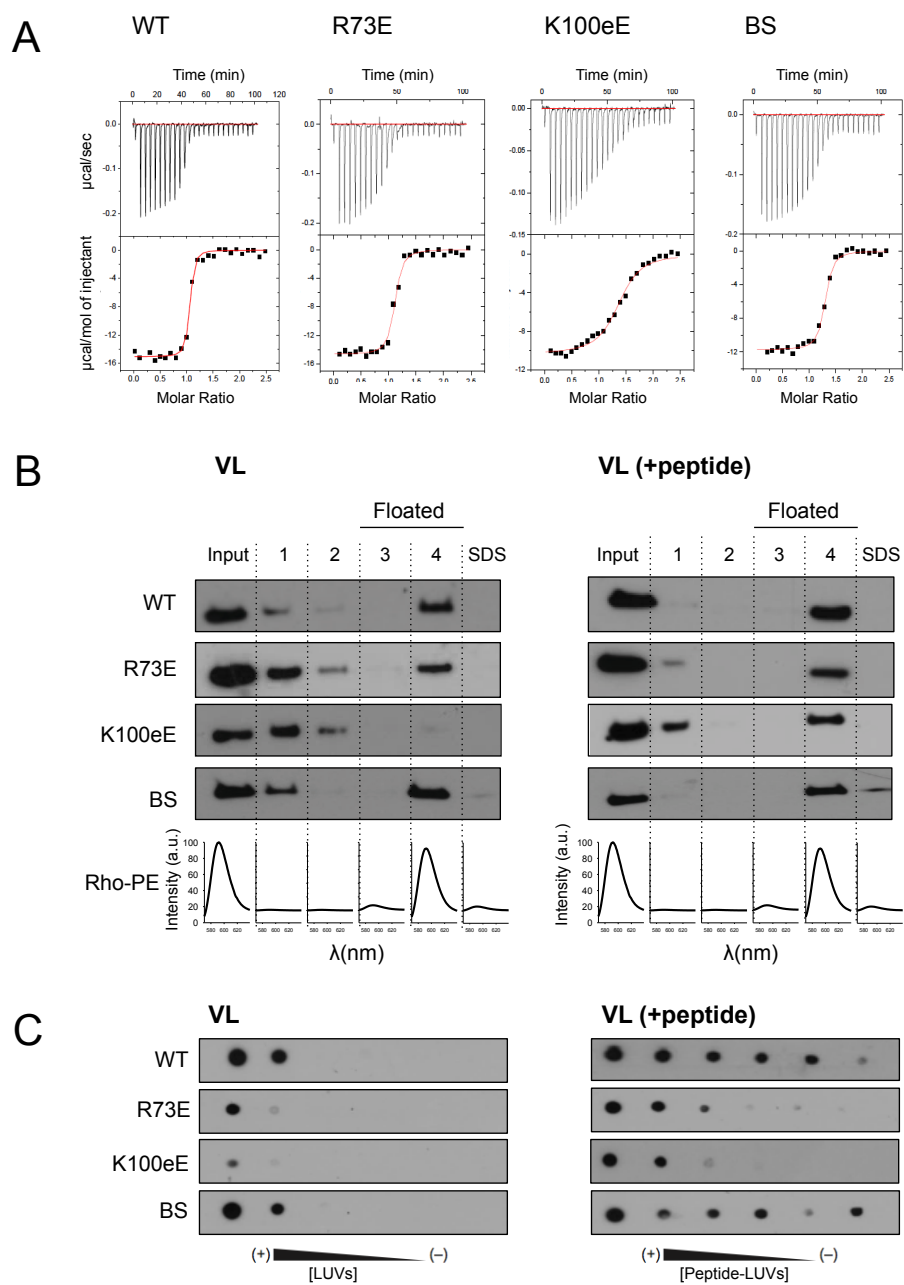


Figure 3

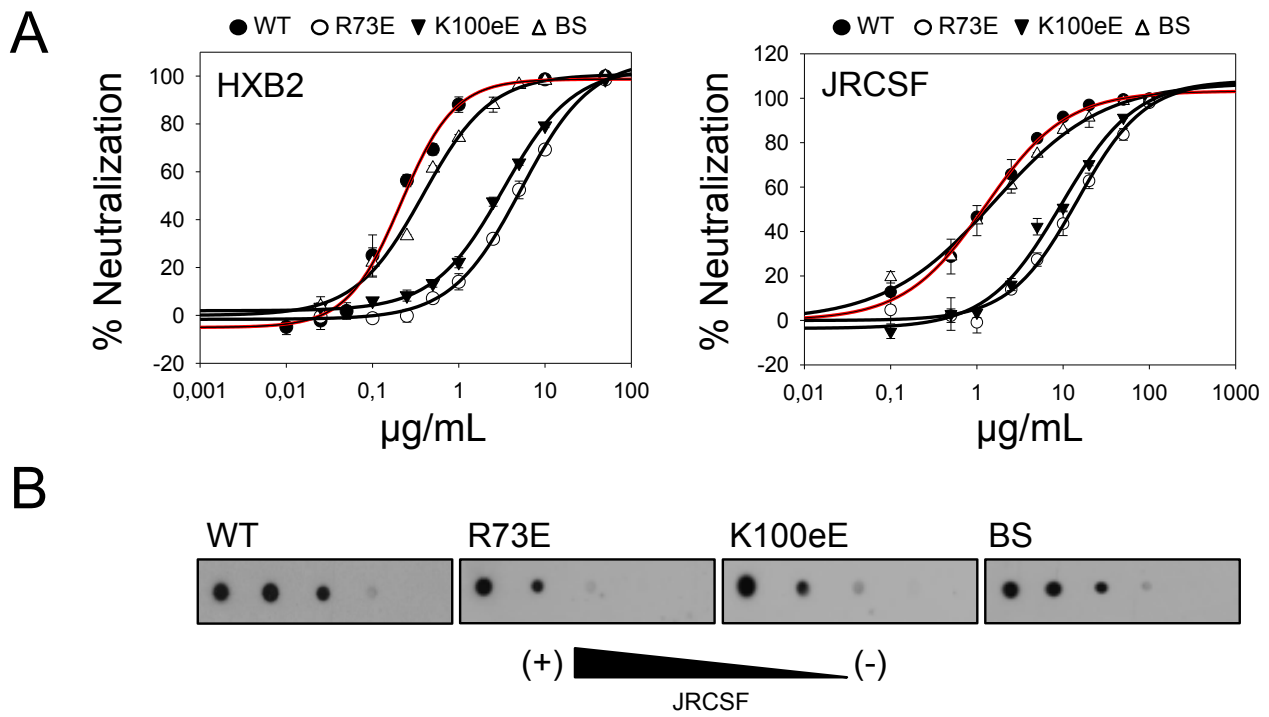


Figure 4

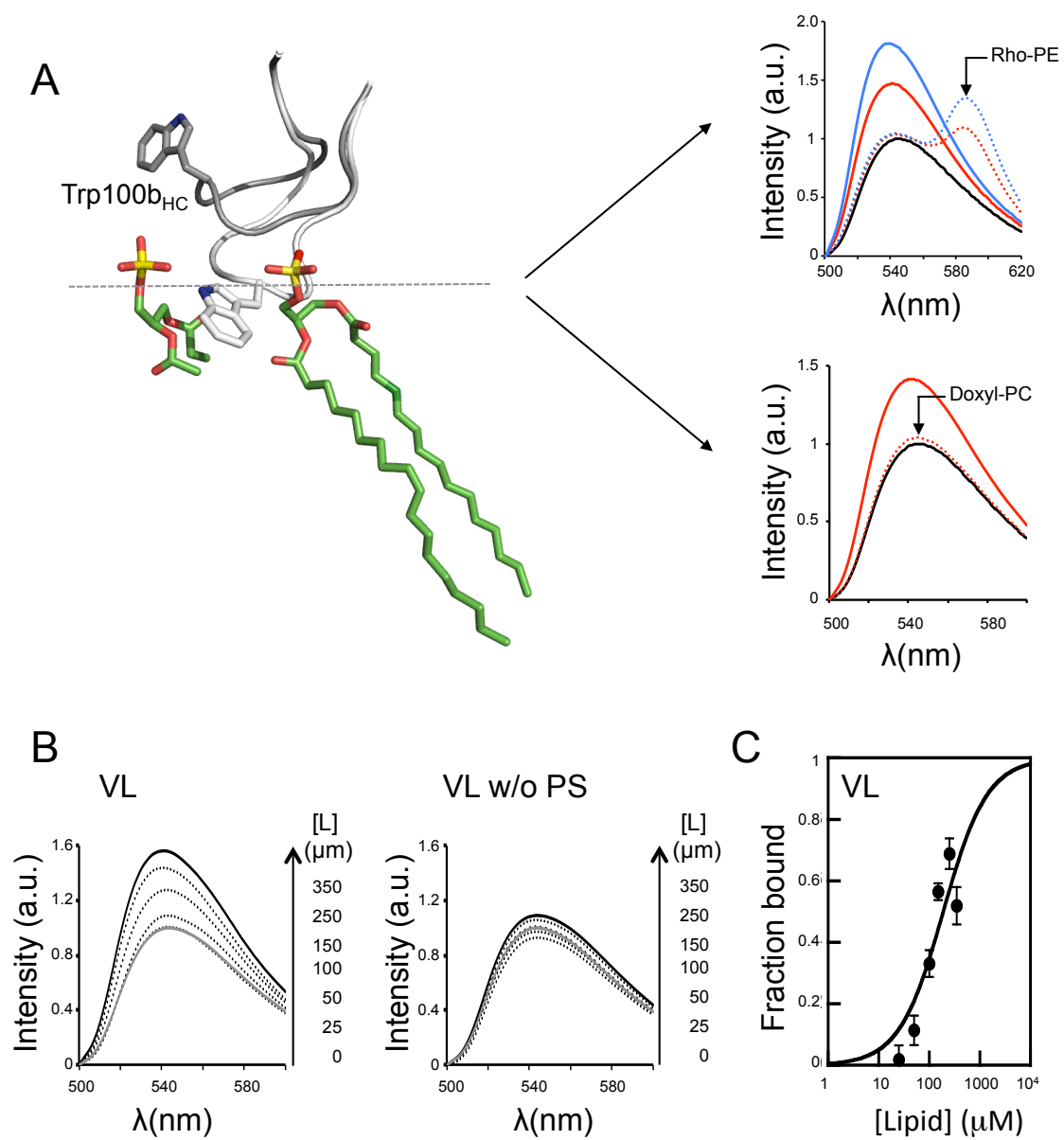


Figure 5

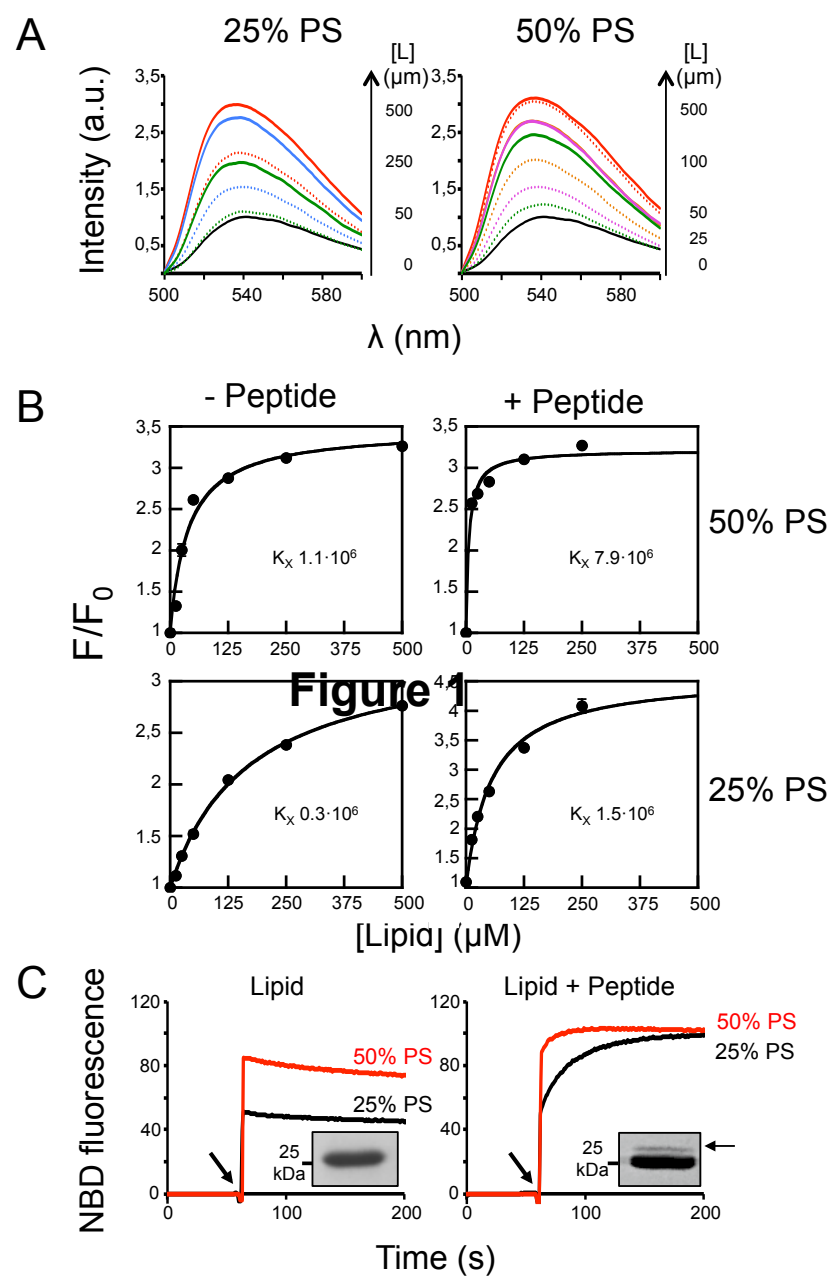


Figure 7

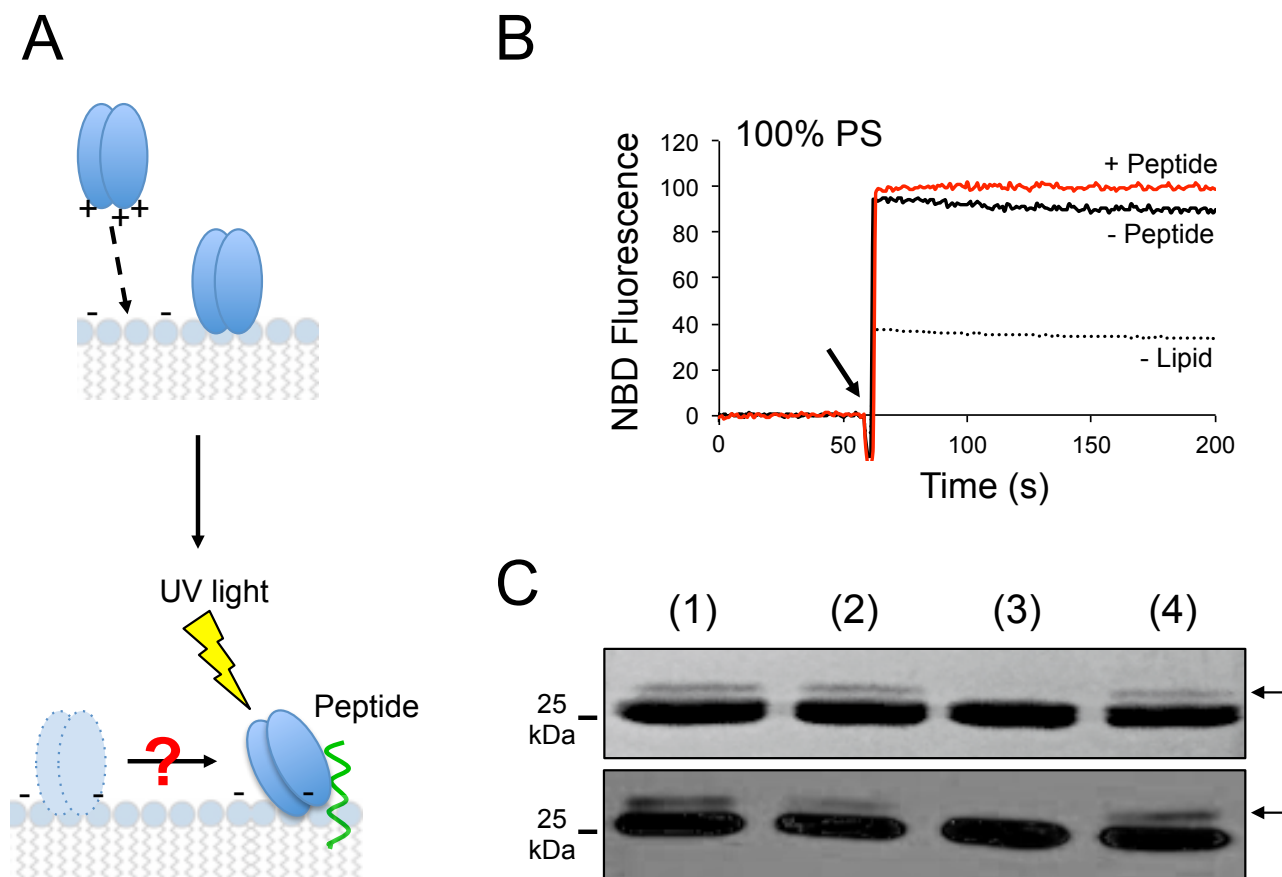


Figure 8

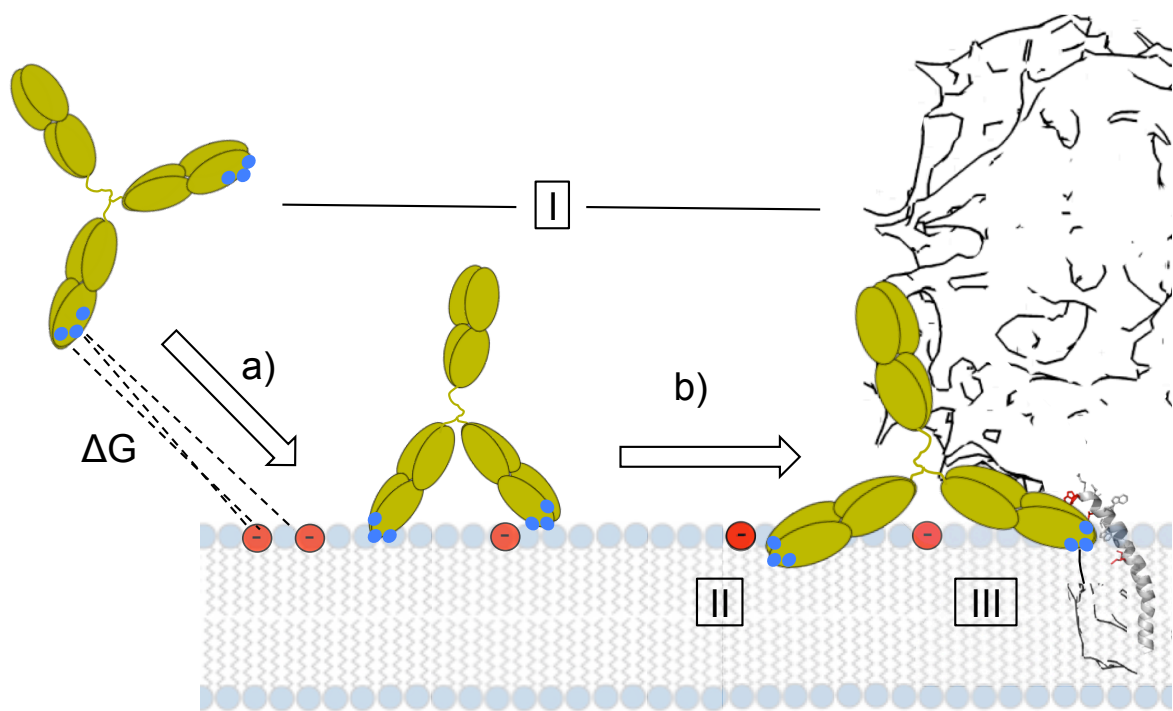


Figure 9